Journal of Materials Chemistry B

Accepted Manuscript

ROYAL SOCIETY OF CHEMISTRY

www.rsc.org/materialsB

The design and synthesis of a soluble composite silica xerogel and the short-time release of proteins

Rong Chen[a, b], Haibo Qu[b], Shaoyun Guo[a*], Paul Ducheyne[b*]

[a] The State Key Laboratory of Polymer Materials Engineering, Polymer Research Institute of Sichuan University, Chengdu, Sichuan 610065, China

[b] Department of Bioengineering, Center for Bioactive Materials and Tissue Engineering, University of Pennsylvania, Philadelphia, PA 19104, USA

* Corresponding author: Prof. Shaoyun Guo, Email: nic7702@scu.edu.cn

Tel: 86-28-85405135

Fax: 86-28-85466077

Prof. Paul Ducheyne, Email: ducheyne@seas.upenn.edu

Tel: 1-215-898 1521

Fax: 1-215-573 2071

Abstract

Conventional silica xerogels prepared through sol–gel processing are regarded as suitable materials for the long-term release of proteins due to the mild processing conditions. However, they fall short of short-time release of these large molecules because of its small pore size and a slow dissolution rate. With the goal of achieving controlled release of large molecules (such as proteins) in a very short time (several days), herein we focus on the co-hydrolysis and co-condensation of different precursors to synthesize composite xerogels (co-xerogels) with adjustable degradation rates. Tetraethoxysilane and 3-(triethoxysilyl) propylsuccinic anhydride were employed to prepare the co-xerogels. Succinic anhydride was chosen for its potential to crosslink with Si-OH and to integrate into the silica network under acidic conditions. Using trypsin inhibitor (TI) as a model drug to characterize the release properties of co-xerogels, we obtained tailored release behavior of TI (2-7 days). It is demonstrated that the co-hydrolysis and co-condensation of different precursors is an easy technique that further expands the applicability of sol–gel materials as excellent carriers for the controlled release of a variety of drugs.

Keywords: silica xerogel, tetraethoxysilane, 3-(triethoxysilyl) propylsuccinic anhydride, soluble matrix

1. Introduction

In recent years, room temperature processed silica based sol–gels have been extensively studied for drug delivery, by virtue of a series of advantages, including biocompatibility, biodegradability, absence of toxicity and easy synthesis procedures[1-7]. Due to the mild processing conditions, high concentrations of many types of biologically active agents can be incorporated in the liquid sol[8-16]. After gelation, the wet gel turns into a solid matrix containing fully interconnected nanopores. The agents are uniformly incorporated within the porous network of the matrix. The resultant material is a gel, and depending on the drying process might be a xerogel or aerogel. Inherent to the sol–gel processing is the flexibility to achieve demanding requirements for different drug release systems[6]. In our laboratory, the controlled release of many molecules from xerogels has been analyzed[17], including antibiotics[11, 18], proteins[9], growth factors[8] and other drugs.

With typical small size of the pores in the xerogel in comparison to the size of drug molecules with large molecular weight, the release of these drugs through diffusion mechanism is greatly impeded. The release arising from xerogel resorption, is typically also slow. For example, when implanted, the xerogel particles resorbed gradually, with 40%-50% reduction in particle size after 4 weeks implantation[19]. As a result, the delivery of large molecules, such as growth factors, for a period of a week or two, cannot be achieved. However, unlike diffusion mechanism that the release kinetics can be adjusted by varying the pore structures of xerogel, few means are available for adjusting the degradation rate of xerogel. As demands for controlled release of large molecules such as growth factors and proteins expand readily, the need for xerogels that can easily adjust degradation rates emerges.

Organically modified alkoxides, such as $RSi(OEt)_3$ (e.g. R=CH_3 or CH_2CH_3), have been used to adjust the drug release kinetics by partially substituting precursor Tetraethoxysilane (TEOS) with the aim to provide hydrophobicity or hydrophilicity to the sol-gel materials. We hypotheses that these modified-groups (R), if unable to react with Si-OH bonds during condensation, create defects in the silica sol-gel network (Figure 1a). The rising number of defects accompanies with less Si-O-Si bond needed for sol-gel to dissolve. As the result, the degradation rate should be greatly affected by the number of defects.

To verify such hypothesis, one need to find a R group of organically modified alkoxide that can either create defects in the xerogel network (Figure 1a) or crosslink to Si-OH bonds during condensation (Figure 1b). Succinic anhydride was selected in this paper by virtue of its tailorable structure in different pH, and as such, different degrees of crosslinking with Si-OH can be obtained. Thus, we choose 3-(triethoxysilyl) propylsuccinic anhydride (TESPSA) to co-hydrolyse and co-condensate with TEOS with the goal to create a composite xerogel (that is, co-xerogel) with adjustable dissolution rate. Figure 2 shows the chemical structure of TESPSA. A cast-drying processing step is also included during the co-condensation, with the aim of adjusting the chemical and morphological structure of co-xerogel[20]. In this study, trypsin inhibitor (TI) was employed as a model drug[9, 21, 22], and it was found that the release rate of TI was significantly affected by the variation of synthesis parameter of co-xerogel, such as molar ratio of precursors and the pH value. With release kinetics obtained, a short-time controlled release of drugs with large molecular size (such as proteins) is possible.

2. Materials and Methods

2.1 Synthesis of co-xerogel

Co-xerogel was prepared at room temperature via a one-step acid catalyzed co-hydrolysis and co-condensation. One milliliter of tetraethoxysilane (TEOS, Strem Chemicals, Newburyport, MA) was combined with 3-(triethoxysilyl) propylsuccinic anhydride (TESPSA, Gelest Inc., Morrisville, PA), to achieve the molar ratios of TEOS/TESPSA of 80/20, 85/15 and 90/10. Then 0.67 ml deionized water (DI) and 0.063 ml of 1N HCl solution were added to the mixture. TEOS, TESPSA, DI and 1N HCl were mixed in a glass vial and stirred with a magnetic stirrer for 2 h to obtain a homogenous sol. Varied amounts of 1N NaOH solution were added into sol to obtain different pH values. After stirring for another 15 min, the sols were cast in a polystyrene (PS) Petri dish, with the diameter of Petri dish being 5.0 cm, and then dried in a 37^{o}C oven.

For the synthesis of TI loaded co-xerogel, TI was first dissolved in 0.1N acetic acid solution at a concentration of 10 mg/ml (the solution would be turbid if the TI concentration exceeded 15 mg/ml), then a uniform and transparent TI solution was obtained. The volumes of TI solution were adjusted when mixed with sol in order to obtain co-xerogels with different TI contents. Subsequently, 1N NaOH solution was slowly added to achieve different pH values. After stirring for another 15 min, the sols were cast in a polystyrene (PS) Petri dish, with the diameter of Petri dish being 5.0 cm, and then dried in a 37^{o}C oven.

After the weight of co-xerogel became constant, the dried co-xerogels were crushed into granules using mortar and pestle, and sieved to retain the fraction with particle size

range of 40-70 μm. Synthesis parameters for different co-xerogels are summarized in Table 1. Our nomenclature for the co-xerogels is, for example, M-85/15-3, meaning the xerogel is prepared under conditions that the molar ratio of TEOS/TESPSA is 85/15, and the pH of the sol is 3; M25-85/15-3, meaning the co-xerogel is prepared under the same conditions as mentioned before, and the drug loading of TI is 25 mg per gram of silicon oxide (mg/g SiO_2).

2.2 Thermogravimetric (TG) analysis

The thermal stability of co-xerogel samples was examined using a TGA Q500 analyzer (TA Instruments, USA). The measurements were taken in nitrogen flow at a heating rate of 10 ^oC /min with temperature range from 20 to 500 ^oC.

2.3 Gas sorption

The nanostructure of the co-xerogels was measured using N_2 (-196^oC) and CO_2 (0^oC) adsorption isotherms. Prior to the analyses, the co-xerogels were outgassed at 120^oC for 24 h. The outgas temperature was set based on the TGA results of co-xerogel, which indicate that 120^oC is the maximum outgas temperature in order to avoid decomposition of silanol groups. After 24 hours outgassing, the vacuum was maintained below 5×10^{-3} torr (0.667Pa).

N_2 adsorption–desorption isotherms were measured at -196^oC using an Autosorb 1 (Quantachrome). Porosity characteristics such as the specific surface areas (SA) and the pore volume (PV) were determined through the multipoint Brunauer–Emmett–Teller (BET) method.

CO_2 adsorption isotherms were measured at 0°C using an ASAP 2020 volumetric adsorption analyzer (Micromeritics, Norcross, GA). The saturation vapor pressure of CO_2 at 0°C was taken as 34.84 bar (3.484 $\times 10^6$Pa). Volume of micropores was calculated using 1.023 g cm^{-3} as the liquid state density for CO_2[23].

2.4 Fourier Transform Infrared Spectroscopy

The Fourier transform infrared spectra (FTIR) of co-xerogels were recorded for the purpose of characterizing the variation of the structure of co-xerogels with different synthesis parameters. The samples were measured on a Nicolet-560 spectrometer (Nicolet Co., USA) at a resolution of 2 cm^{-1} with accumulation of 32 scans in the spectral range of 4000-400cm^{-1}.

2.5 X-ray Photoelectron Spectra

The X-ray photoelectron spectra (XPS) of co-xerogels were collected on a Vacuum Generators KRATOS XSAM800 spectrometer (Kratos Corp., UK) using AlKα source (hv=1486.6 ev). Correction of the energy shift due to static charging of the samples was accomplished by referencing to the C1s line from the residual pump line oil contamination, taken at 284.8 eV. A pressure of 5×10^{-7} Pa was maintained during the analysis.

2.6 Weight loss

The weight loss of co-xerogels during immersion was measured for up to 7 days using 50 mg of sample incubated in 10 ml tris(hydroxymethyl)aminomethane buffer solution ($(CH_2OH)_3CNH_2$, tris buffer for short, Sigma Chemical Co., St. Louis, MO) (pH 7.6 @

37°C) at 37°C in a Series II Water Jacketed CO_2 incubator (Thermo Forma, Marietta, Ohio) at 100 rpm. After immersion for certain days, the co-xerogels were vacuum dried at 40 °C until the weight was constant. The weight of co-xerogels after immersion was measured, and the weight loss was calculated as follows:

$$\text{Weight loss}(\%)=\frac{W_0 - W_1}{W_0}\times 100\% \qquad (1)$$

where W_o is the weight of original co-xerogel, and W_1 is the weight of immersed co-xeorgel.

2.7 *In vitro* drug release

In vitro drug release from co-xerogels was measured for up to 7 days using 75 mg of sample incubated in 15 ml tris buffer solution at 37°C in a Series II Water Jacketed CO_2 incubator at 100 rpm. The buffer solution, free of inorganic ions, was used to minimize electrolyte interference with the protein measurements[22]. At each time period selected for measurement (24, 48, 72, 96, 120, 144 and 168 h), the solution was totally exchanged. All experiments were performed in triplicate. The concentrations of protein were measured using a gold colloidal assay (Intergrated Separation Systems, Natick, MA) through an ultraviolet-visible spectrophotometry (Ultraspec Plus, Pharmacia LKB, Piscataway, NJ), with the wavelength set at 595 nm[22]. A standard calibration curve for TI was prepared at concentrations ranging from 0.5 μg/ml to 20 μg/ml. These curves exhibited linear behavior over the full range of concentration. If the TI concentration of collected solution exceeded 20 μg/ml, the solution was first diluted (to range of 0.5-20 ug/ml), measured, and then multiplied with the dilution ratio.

3. Results

3.1 Thermogravimetric (TG) analysis

Figure 3 shows the TG curves for the thermal stability of different co-xerogels at a heating rate of 10 ^{o}C/min under a nitrogen atmosphere. The TG curves of co-xerogels have two distinct stages. The initial weight loss of about 4.0% in the range of 40-120 ^{o}C could be attributed to the evaporation of adsorbed water molecules[24, 25]. After that, a continuous weight loss occurred, possibly due to the dehydroxilation, i.e. conversion of silanol to form siloxane groups[26, 27].

3.2 Gas sorption analysis

The nanostructural properties, namely the specific surface area (SA) and the pore volume (PV) for co-xerogels obtained from the N_2 adsorption isotherms at -196 ^{o}C are shown in Table 2. The SA and PV values of co-xerogels were barely measurable, demonstrating that a dense structure was formed. For co-xerogels with different molar ratios of TEOS/TESPSA and different pH values, the SA and PV were similar, demonstrating again that few pores were generated for co-xerogels using various synthesis conditions. The limited porosity in this study was the result of rapid drying during the condensation, and similar result was reported by us[21].

To further investigate the microporosity of co-xerogel, CO_2 adsorption isotherm at 0^{o}C was performed. Although the critical dimension of the CO_2 molecule (0.28 nm) is similar to that of N_2 (0.30 nm), the higher adsorption temperature used in CO_2 adsorption compared with that for N_2 enables a higher kinetic energy of the molecules, which

overcomes the restriction of CO_2 diffusing into pores narrower than 0.5 nm[26, 27]. Fig. 4 shows a CO_2-adsorption isotherm that covers relative pressures up to 0.03, because working pressures were below 1 atm. The micropore volume of M-85/15-3, calculated using NLDFT method[28], is 0.007 cm^3/g. The CO_2 adsorption result (0.007cm^3/g) is in accordance with the N_2 adsorption result (0.001cm^3/g), indicating a dense microstructure of co-xerogel obtained in this study.

3.2 Chemical structure of the co-xerogel

The FTIR spectra of co-xerogels with different synthesis parameters (pH value and molar ratio of TEOS/TESPSA) are shown in Figure 5. In accordance with the data reported earlier[10, 29], the peaks at 1082 cm^{-1} and 1250 cm^{-1} are caused by the asymmetric stretching vibrations of Si–O–Si, while the peak at 800 cm^{-1} is caused by the symmetric stretching vibrations of Si–O–Si[10, 29]. The absorption band at 939 cm^{-1} is related to the vibration of Si–OH bonding[30], and the presence of absorbed water in all studied silica xerogels is indicated by the OH bands at 3750–3000 cm^{-1}. The absence of FTIR peaks at 1810 $cm^{-1}$and 1710 cm^{-1}, which correspond to the symmetric and asymmetric stretching vibrations of the anhydride group, indicates that the anhydride group of TESPSA is fully hydrolyzed. Fig 5(a) shows that no new absorption peak appear for co-xerogels synthesized at lower pH value (pH=1 and 3), while new peaks at 1580 cm^{-1} and 1420 cm^{-1} observed at higher pH (pH=5 and 7). These peaks correspond to the symmetric and asymmetric stretching vibrations of C=O from COO^-[31, 32]. After the normalization of these FTIR data in the range of 2000 cm^{-1}–1400 cm^{-1}, it is observed that the peak intensity at 1720 cm^{-1} became lower with higher synthesis pH, which is corresponding to the stretching vibrations of C=O from undissociated –COOH or –CO-O-Si. At the same

time, the peak intensity at 1580 cm^{-1} increased with higher synthesis pH, which is corresponding to the stretching vibrations of C=O from COO^-.

For co-xerogels with different molar ratio of TEOS/TESPSA, although no new absorption peaks were observed with the variation of molar ratio (Fig 6), the intensity of peak at 1720 cm^{-1}, caused by the stretching vibrations of C=O from hydrolyzed anhydride group[32-34], increased with the increase of TESPSA content.

The FTIR spectra of co-xerogels were investigated at different immersion time, with the aim to study the structure variation of co-xerogels after different immersion times (Fig. 7). New peaks at 1580 cm^{-1} and 1420 cm^{-1} can be observed upon immersion. These peaks also correspond to the symmetric and asymmetric stretching vibrations of C=O from COO^-.

The chemical structure of co-xerogels was further analyzed by XPS. The XPS spectra of binding energies of Si 2p and O 1s of co-xerogels with different pH values and molar ratios of TEOS/TESPSA are shown in Fig. 8. From the Si 2p spectrum (Fig. 8a, b and c), the binding energy at 103.3 eV corresponds to the Si atoms in Si-O group within the co-xerogel matrix. This is in accordance with previous data[35]. The binding energy of the principal O 1s (Fig. 8d, e and f) for the co-xerogels can be deconvoluted into two contributions: one at 533.0 eV, assigned to the O atoms in Si-O group within the co-xerogel matrix and the possible C-O group corresponding to the unhydrolyzed Si-O-C_2H_5 group in TEOS and TESPSA, and the other at 532.0 eV, associated with C=O group within the TESPSA chain[36].

In order to verify the structure variation of co-xerogels during the co-hydrolysis and co-condensation, the XPS spectra of C 1s is shown in Fig. 8g, h and i, at different pH values and molar ratios of TEOS/TESPSA. For co-xerogels at lower pH (that is, M-85/15-3), the binding energy of C 1s was situated as three levels: the binding energy at 284.8 eV corresponds to the C atoms in C-C group, the binding energy at 286.0 eV corresponds to the C atoms in C-O group, and the binding energy at 289.1 eV corresponds to the C atoms in O=C-O group[37]. The variation of molar ratio of TEOS/TESPSA (M-80/20-3) had little effect on the location of the C 1s peaks, while a new peak was observed at 287.7 eV at higher pH (M-85/15-7). This peak could be assigned to the C atoms in $-COO^{-}Na^{+}$ group[38].

3.3 Dissolution behavior

The weight loss of co-xerogels synthesized at different pH values and molar ratios of TEOS/TESPSA is shown in Table 3 and Figure 9. All the samples were immersed in tris buffer for 7 days. When the pH value is constant (pH=3), the solubility of co-xerogel increased with greater molar content of TESPSA: the weight loss varied from 21.7 ±1.9% to 87.9 ±3.3% as the molar ratio of TEOS/TESPSA changed from 90/10 to 80/20. For the co-xerogels with the same molar ratio of TEOS/TESPSA (85/15), the solubility of co-xerogels increased with the increase of pH value of the mixed sol. That is, the weight loss after 7 days immersion increased from 38.7 ±1.8% to 59.5 ±1.9% when the pH value increased from 1 to 7.

3.4 Drug release

The effect of synthesis parameters (such as pH value and molar ratio of TEOS/TESPSA) on the release of TI from co-xerogels is shown in Fig. 10, with the drug loading being 25 mg/g SiO_2. It was found that the prorated released amount was pH dependent and increased with higher pH (Fig. 10a). More than 90% TI was released after 5 days immersion when the pH value was 7 and 5, while 80% TI was released after immersed for 7 days when synthesized at lower pH (pH=1).

Meanwhile, the released amount of TI (in %) decreased with lower content of TESPSA. When the molar ratio of TEOS/TESPSA varied from 80/20 to 90/10, the amount of TI released in the first 48 h decreased from 90 to 9.1 % (Fig. 10b). A linear release curve was obtained for co-xerogels with a molar ratio of TEOS/TESPSA at 90/10.

4. Discussion

Compared to a conventional acid catalyzed sol-gel process with a single alkoxysilane precursor, the synthesis of a co-xerogel based on TEOS and TESPSA went through the co-hydrolysis and co-condensation of these two precursors, and consequently, exhibited some unique phenomena and properties. It is useful to first determine the synthesis mechanism of the co-xerogel. With this knowledge, the dissolution properties then can be easily varied by modifying the synthesis parameters.

With reference to figure 11, the formation of co-xerogel at different pH values can be explained as followed. During the co-hydrolysis, the anhydride group of TESPSA is activated and hydrolyzed by the HCl acid catalysis. The degree of crosslinking of hydrolyzed anhydride group and Si-OH varies under different synthesis pH. At lower pH

values (pH=1 or 3), new crosslink points are produced through the reaction between that and Si-OH (hydrolyzed through TEOS), evidenced by the presence of –CO-O-Si (with band at 1720cm^{-1}). At higher pH values (pH=5 or 7), the hydrolyzed anhydride of TESPSA is presented as –COO$^-$, evidenced by the emergence of band at 1580cm^{-1}, which is stable in the co-condensation processing. This decreases the extent of crosslinking in the co-xerogel by virtue of the repulsion of like-charged particles. To illustrate the pH effect on the degree of crosslinking of hydrolyzed anhydride group, Table 4 summarizes the FTIR analysis for the anhydride group's evolution under different pH.

Focusing on the C 1s XPS data (Fig. 8), a new peak appeared at 287.7 eV for samples catalyzed at higher pH values (M-85/15-7). This suggests that –COO$^-$ groups were generated when pH value was 7.

The degree of crosslinking of hydrolyzed anhydride group and Si-OH affects the degradation rate of co-xerogels. Weight loss measurement of the co-xerogels after 7 days of immersion exhibited different solubility at different molar ratios of TEOS/TESPSA and pH values (Table 3). The weight loss increases for co-xerogels prepared under higher pH value, coinciding with a lower degree of crosslinking (of Si-R-Si) under higher pH (Fig. 11) as revealed by FTIR results (Fig. 5). The solubility was also enhanced with the increase of molar content of TESPSA, which was also due to less crosslink points. During degradation, in addition to the breakup of Si-O-Si bonds, the crosslinked –CO-O-Si also underwent hydrolysis. The appearance of 1583 cm^{-1} peak after several days' of immersion indicates the disintegration of –CO-O-Si and formulation of the -COO$^-$ (Fig. 7).

Plotting the weight loss and TI release data together (Fig. 12), we observed a period where the percentage of drug release and weight loss overlapped at lower synthesis pH (1, 3 and 5) and the duration of that period decreased as the pH increases. It suggests that the drug release is degradation-controlled in the initial stage. The dissolution of co-xeorgel generated more defects (-COO^-) by breaking the bond of –CO-O-Si in the matrix, which enabled the additional release of TI through diffusional mechanism. Thus, the release scheme gradually switches to be controlled by both degradation and diffusion. While for co-xerogels with higher pH (M-85/15-7), large numbers of defects (-COO^-), due to a lower degree of crosslinking, existed in the matrix, which induced the diffusional release of TI at the beginning of the immersion. It is interesting to note that there is a complete release when the co-xerogel has been degraded only by a 40-60 %. The reason could be the formation of release channel for TI during the immersion. That is, lots of pores were formed due to the degradation of co-xerogel. The subsequent TI diffusion through the newly formed porous structures in the silica matrix becomes a second release mechanism in addition to the degradation controlled release. This phenomenon has been well documented in the previous work[39]. As a result, TI released almost completely when the xerogel degraded only 40-60%.

TI was chosen as the model drug in this study, as it has been used as a model protein in a number of studies [40, 41]. Many difficult-to-treat diseases can benefit from controlled delivery of growth factor, particularly in treating large bone defects where growth factors such as BMP-2, PDGF are needed to accelerate bone repair processes [42-47]. In this study, we did not vary the particle size, but chose to focus on the fundamental aspect of degradation behavior. Co-xerogel particles, suspended in saline solution, can be

administered into the bone defect by injection through medical syringe needles. The 40-70 μm size of particles was used, as grinding to this particle size is very reproducible in a lab setting and such size.

5. Conclusions

In order to achieve the excellent loading and controlled release of large molecular drugs (such as proteins), TEOS and TESPSA were selected as precursors to prepare a soluble co-xerogel. The co-hydrolysis and co-condensation of these two silica precursors was achieved, and the solubility of co-xerogel can be easily adjusted through the variation of experimental parameters such as molar ratio of TEOS/TESPSA and the pH value of the mixed sol. The extent of crosslinking of the co-xerogels, influenced by the synthesis pH values, controls the solubility of co-xerogel and the release kinetics. A short-time release of protein (Trypsin Inhibitor as model drug) (2-7 days) was obtained.

Acknowledgments

The authors gratefully acknowledge the support from U.S. Army Medical Research and Materiel Command contract # W81XWH-10-2-0156, the National Natural Science Foundation of China (21174091 and 51303111) and Funds for Doctoral Disciplines of The Ministry of Education of China (20130181120122).

References

1. P. Ducheyne and Q. Q. Qiu, Biomaterials., 1999, **20**, 2287-2303.
2. Z. Z. Li, L. X. Wen, L. Shao and J. F. Chen, J. Control. Release., 2004, **98**, 245-254.
3. U. Maver, A. Godec, M. Bele, O. Planinsek, M. Gaberscek, S. Srcic and J. Jamnik, Int. J. Pharmaceut., 2007, **330**, 164-174.
4. D. Quintanar-Guerrero, A. Ganem-Quintanar, M. G. Nava-Arzaluz, E. Piñón-Segundo, Expert. Opin. Drug. Del., 2009, **6**, 485-498.
5. I. I. Slowing, J. L. Vivero-Escoto, C-W. Wu, VS-Y. Lin, Adv. Drug. Deliver. Rev., 2008, **60**, 1278-1288.
6. S. Radin, T. Chen, P.Ducheyne, Biomaterials., 2009, **30**, 850-858.
7. H. S. Park, C. W. Kim, H. J. Lee, J. H. Choi, S. G. Lee, Y. Yun, I. C. Kwon, S. J. Lee, S. Y. Jeong and S. C. Lee, Nanotechnology., 2010, **21**, 1-9.
8. S. B. Nicoll, S. Radin, E. M. Santos, R. S. Tuan and Ducheyne P, Biomaterials., 1997, **18**, 853-859.
9. E. M. Santos, S. Radin and P. Ducheyne, Biomaterials., 1999, **20**, 1695-1700.
10. S. Falaize, S. Radin and P. Ducheyne, J. Am. Ceram. Soc., 1999, **82**, 969-976.
11. S. Radin, P. Ducheyne, T. Kamplain and B. Tan, J. Biomed. Mater. Res., 2001, **57**, 313-320.
12. J. Yao, S. Radin, P. S. Leboy and P. Ducheyne, Biomaterials., 2005, **26**, 1935-1943.
13. M. Prokopowicz, Drug. Deliv., 2007, **14**, 129-138.
14. M. C. Costache, H. Qu, P. Ducheyne and D. I. Devore, Biomaterials., 2010, **31**, 6336-6343.
15. K. Czarnobaj, Polym. Bull., 2010, **66**, 223-237.
16. M. Prokopowicz, J. Pharm. Pharmacol., 2010, **59**, 1365-1373.

17. S. Radin and P. Ducheyne, in *Learning from Nature How to Design New Implantable Materials,* ed. R. L. Reis and S. Weiner, Kluwer Academic Publishers, Netherland, 2004, pp. 59-74.
18. W. Aughenbaugh, S. Radin and P. Ducheyne, J. Biomed. Mater. Res., 2001, **57**, 321-326.
19. S. Radin, G. El-Bassyouni, E. J. Vresilovic, E. Schepers and P. Ducheyne, Biomaterials., 2005, **26**, 1043-1052.
20. A. S. Kåss, ØT. Førre, M. W. Fagerland, H. C. Gulseth, P. A. Torjesen and I Hollan, Scand. J. Rheumatol., 2014, **43**, 22-27.
21. R. Chen, H. Qu, A. Agrawal, S. Guo, P. Ducheyne, J. Mater. Sci-Mater. M., 2013, **24**, 137-146.
22. E. M. Santos, S. Radin and P. Ducheyne. Biomaterials., 1999, **20**, 1695-1700.
23. J. C. Echeverría, J. Estella, V. Barbería, Javier Musgo and Julián J. Garrido, J. Non-Cryst. Solids., 2010, **356**, 378-382.
24. Z. W. He, C. M. Zhen, X. Q. Liu, W. Lan, D. Y. Xu and Y. Y. Wang, Thin. Solid. Films., 2004, **462-463**, 168-171.
25. J. C. D. Costa, G. Q. Lu and V. Rudolph, Colloid. Surface. A., 2001, **179**, 243-251.
26. Z. W. He, C. M. Zhen, X. Q. Liu, W. Lan, D. Y. Xu and Y. Y. Wang, Thin. Solid. Films., 2004, **462-463**, 168-171.
27. J. C. D. Costa, G. Q. Lu and V. Rudolph, Colloid. Surface. A., 2001, **179**, 243-251.
28. E. I. Páez, M. Haro, E. J. Juárez-Pérez, R. J. Carmona, J. B. Parra, R. L. Ramos, and C. O. Ania, Mesopor. Mater., 2014, http://dx.doi.org/10.1016/j.micromeso.2014.10.033.

29. C. M. Stoscheck, Anal. Biochem., 1987, **160**, 301-305.
30. S. Radin, S. Falaize, M. H. Lee and P. Ducheyne, Biomaterials., 2002, **23**, 3113-3122.
31. U. Kalapathy, A. Proctor and J. Shultz, Bioresource. Technol., 2000, **73**, 257-262.
32. Y. Liu, in *Spectroscopic Analysis*, Sichuan University Publisher, Chengdu, 2004, pp. 54-98 (in Chinese).
33. A. I. Barabanova, T. A. Pryakhina, E.S. Afanas'ev, B. G. Zavin, Y. Vygodskii, A. A. Askadskii, O. E. Philippova and A. R. Khokhlov, Appl. Surf. Sci., 2012, **258**, 3168-3172.
34. X. Huang, A. Schmucker, J. Dyke, S. M. Hall, J. Retrum, B. Stein, N. Remmes, D. V. Baxter, B. Dragnea and L. M. Bronstein, J. Mater. Chem., 2009, **19**, 4231-4239.
35. Y. Shiina and A. Morikawa, React. Funct. Polym., 2011, **71**, 85-94.
36. R. Mariscal, M. López-Granados, J. L. G. Fierro, J. L. Sotelo, C. Martos, R. V. Grieken, Langmuir., 2000, **16**, 9460-9467.
37. J. Santos, T. H. Ban, T. Teranishi, T. Uozumi, T. Sano and K. Soga, Appl. Catal. A-Gen., 2001, **220**, 287-302.
38. N. Moussa, A. Ghorbel, P. Grange, J. Sol-Gel. Sci. Tech., 2005, **33**, 127-132.
39. S. Radin, S. Bhattacharyya, P. Ducheyne, Nanostructural control of the release of macromolecules from silica sol–gels. Acta. Biomater., 2013, **9**, 7987-7995.
40. A. W. Johnson, N. J. Serrano, A. W. Morgan, R. Jamison, Y. B. Choy, H. Choi, K. Kim and F. DeCarlo, Macromol. Symp., 2005, **227**, 295-305.
41. M. Sutter, J. Siepmann, W. E. Hennink and W. Jiskoot, J. Control. Release., 2007, **119**, 301-312.

42. K. Kleinschmidt, F. Ploeger, J. Nickel, J. Glockenmeier, P. Kunz and W. Richter, Biomaterials., 2013, **34**, 5926-5936.

43. T. Kawasaki, Y. Niki, T. Miyamoto, K. Horiuchi, M. Matsumoto, M. Aizawa and Y. Toyama, Biomaterials., 2010, **31**, 1191-1198.

44. M. D. Schofer, L. Tünnermann, H. Kaiser, P. P. Roessler, C. Theisen, J. T. Heverhagen, J. Hering, M. Voelker, S. Agarwal, T. Efe, S. Fuchs-Winkelmann and J. R. J. Paletta, J. Mater. Sci-Meter. M., 2012, **23**, 2227-2233.

45. Y. Zhang, N. Cheng, R. Miron, B. Shi and X. Cheng, Biomaterials., 2012, **33**, 6698-6708.

46. S. Yamano, K. Haku, T. Yamanaka, J. Dai, T. Takayama, R. Shohara, K. Tachi, M. Ishioka, S. Hanatani, S. Karunagaran, K. Wada and A. M. Moursi, Biomaterials., 2014, **35**, 2446-2453.

47. B. De la Riva, E. Sánchez, A. Hernández, R. Reyes, F. Tamimi, E. López-Cabarcos, A. Delgado, C. Vora, J. Control. Release., 2010, **143**, 45-52.

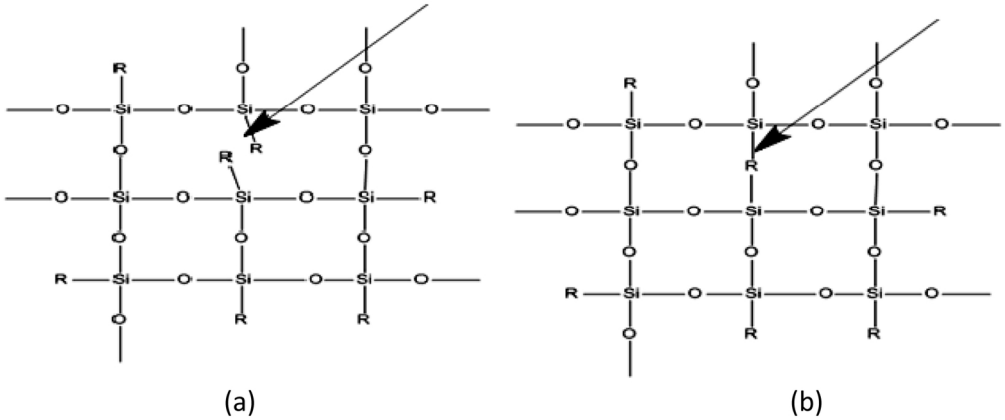

Fig. 1 The condensation reaction for silica precursors with partially substituted R group to (a) create defects in the silica sol-gel network, (b) form crosslink structure in the silica sol-gel network.
69x28mm (600 x 600 DPI)

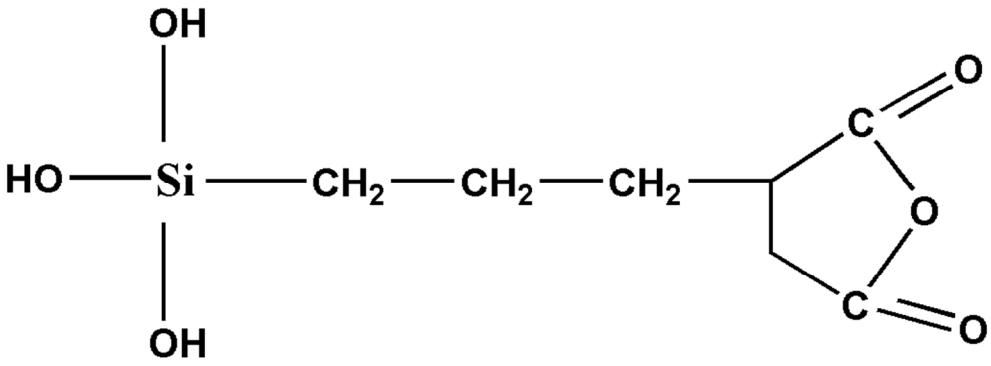

Fig. 2 The chemical structure of TESPSA.
88x32mm (300 x 300 DPI)

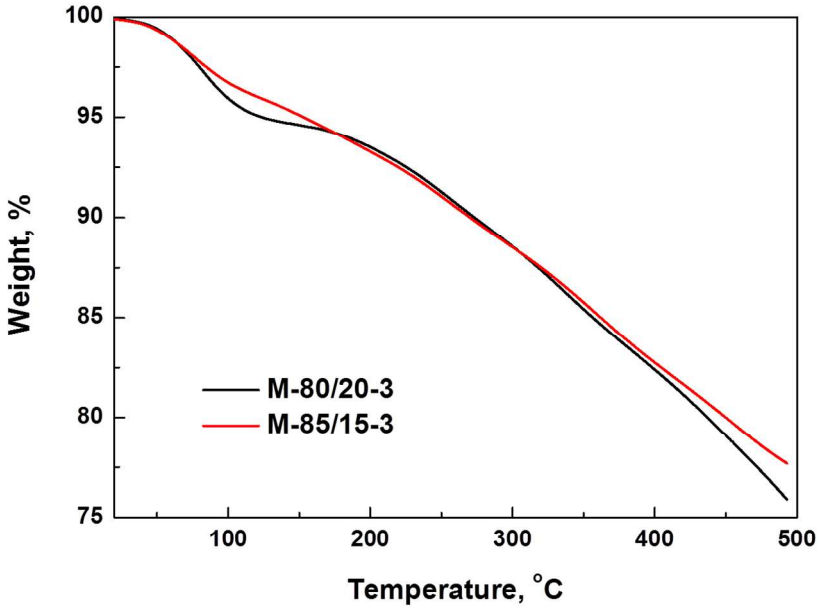

Fig. 3 The thermogravimetric analysis of different co-xerogels.
270x189mm (150 x 150 DPI)

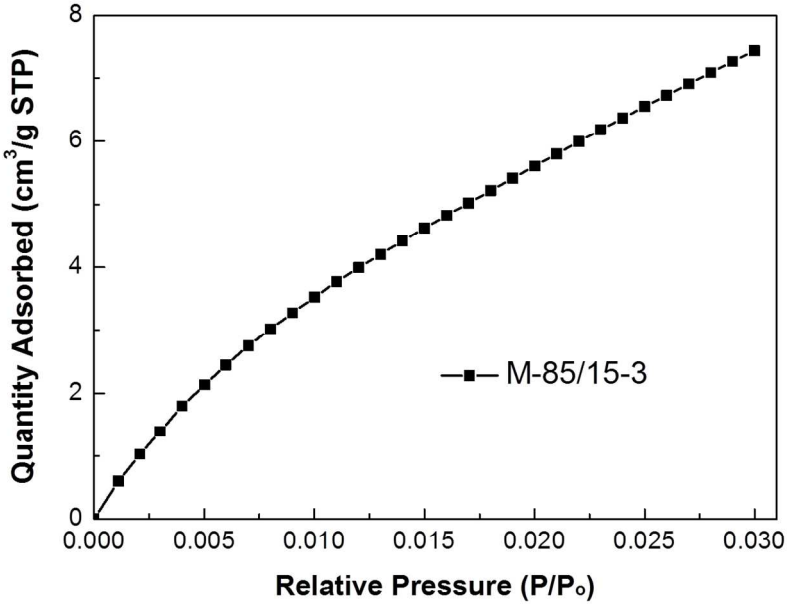

Fig. 4 CO_2 adsorption isotherm on M-85/15-3 at 0°C
273x192mm (150 x 150 DPI)

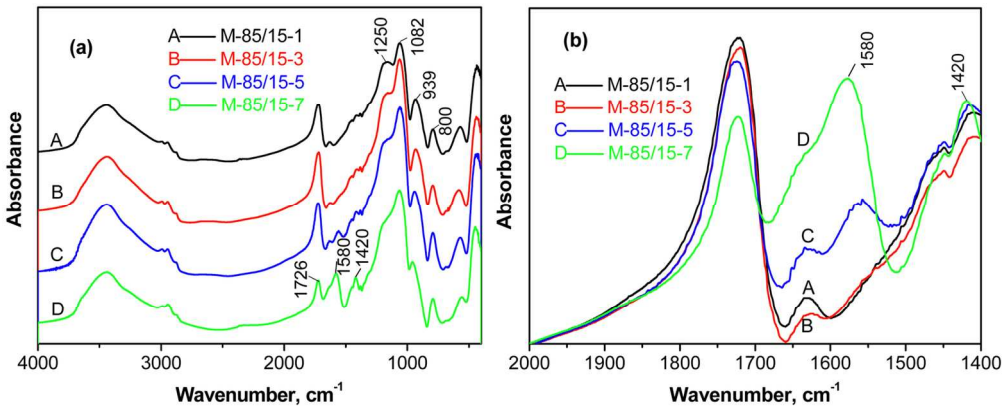

Fig. 5 FTIR of co-xerogel with different pH (a) and the comparison of C=O group after normalization (b).
69x28mm (600 x 600 DPI)

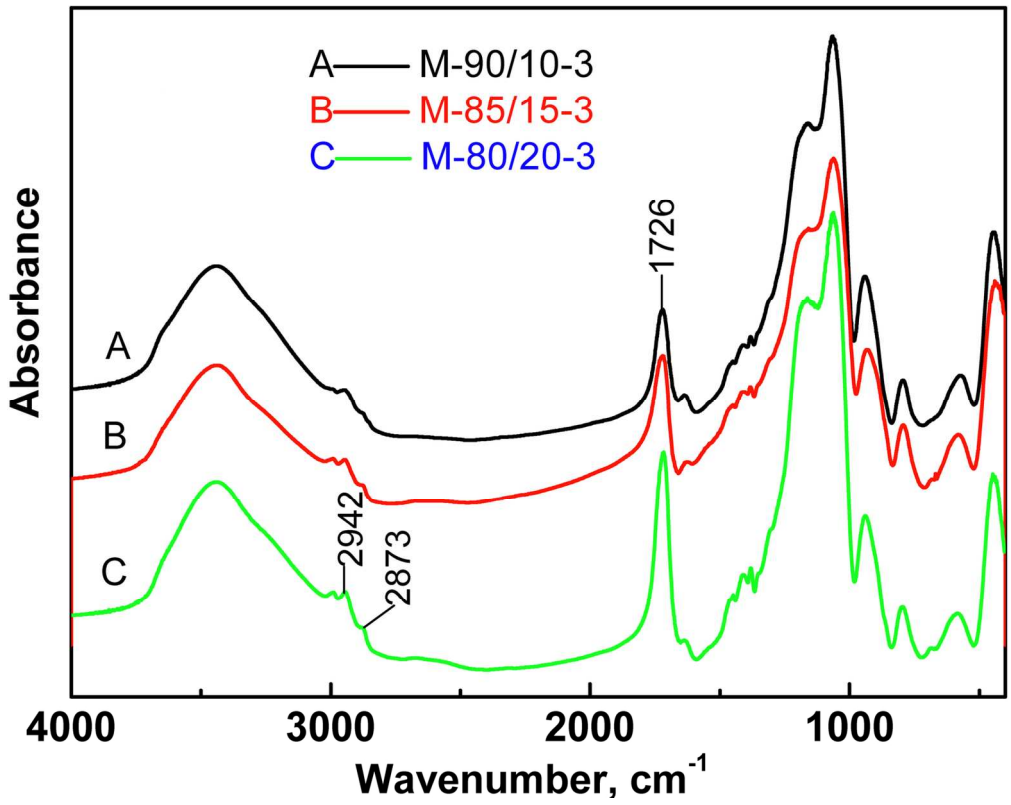

Fig. 6 FTIR of co-xerogel with different molar ratio of TEOS and TESPSA.
70x56mm (600 x 600 DPI)

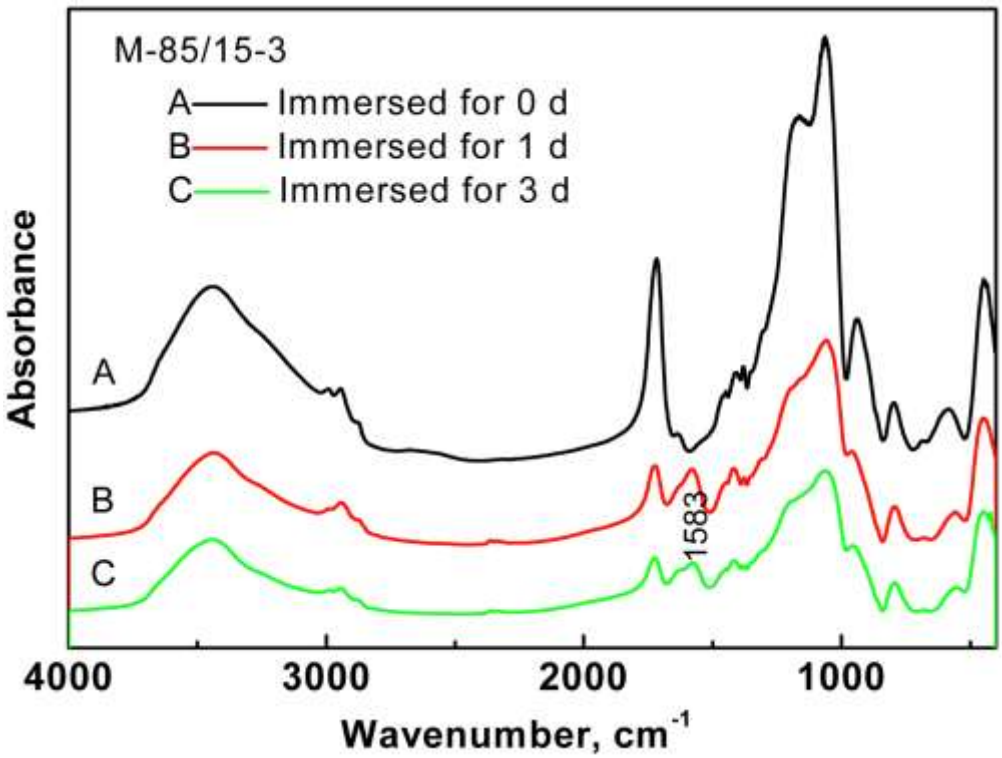

Fig. 7 FTIR for co-xerogels (M-85/15-3) after immersed for different time.
67x50mm (600 x 600 DPI)

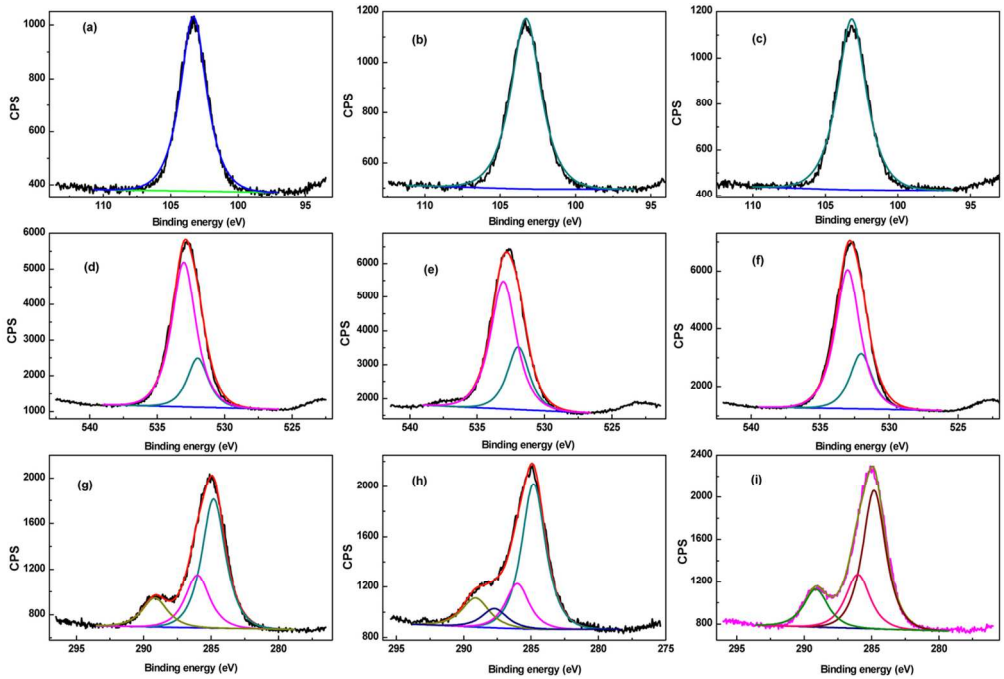

Fig. 8 XPS deconvolution spectra of Si 2p, O 1s and C 1s signals of co-xerogels with different pH value and molar ratio of TEOS/TESPSA. Si 2p signals: (a): M-85/15-3, (b): M-85/15-7, and (c): M-80/20-3; O1s signals: (d): M-85/15-3, (e): M-85/15-7, and (f): M-80/20-3; C 1s signals: (g): M-85/15-3, (h): M-85/15-7, and (i): M-80/20-3.
58x39mm (600 x 600 DPI)

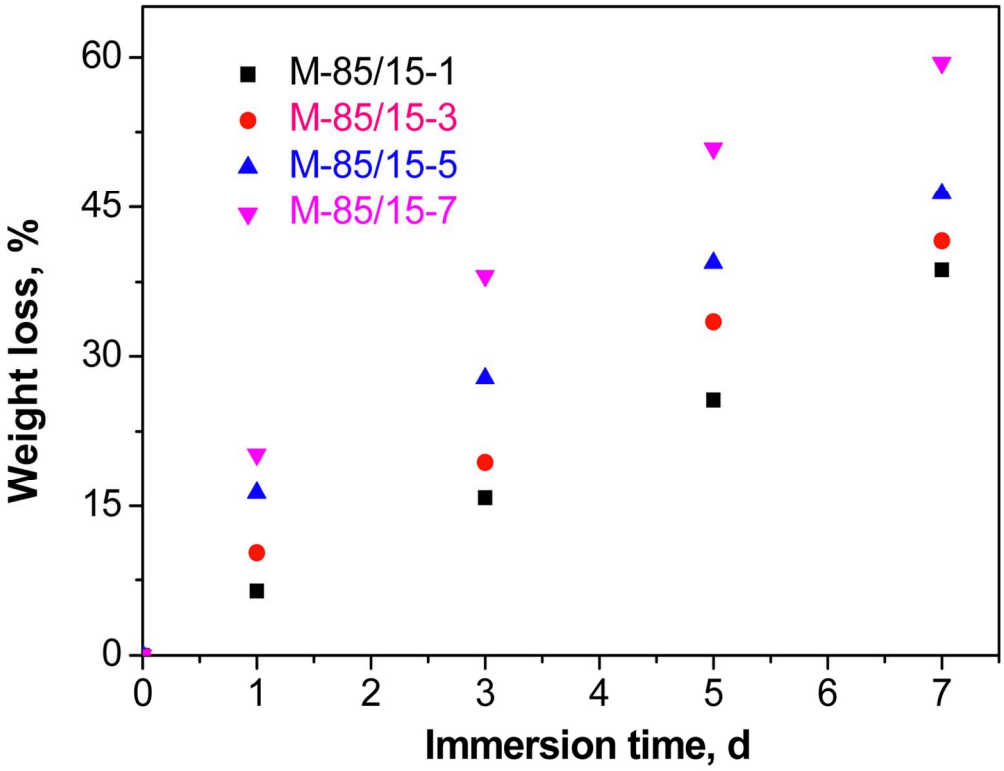

Fig. 9 The effect of immersion time on the weight loss of co-xerogel at different catalysis pH values
63x49mm (600 x 600 DPI)

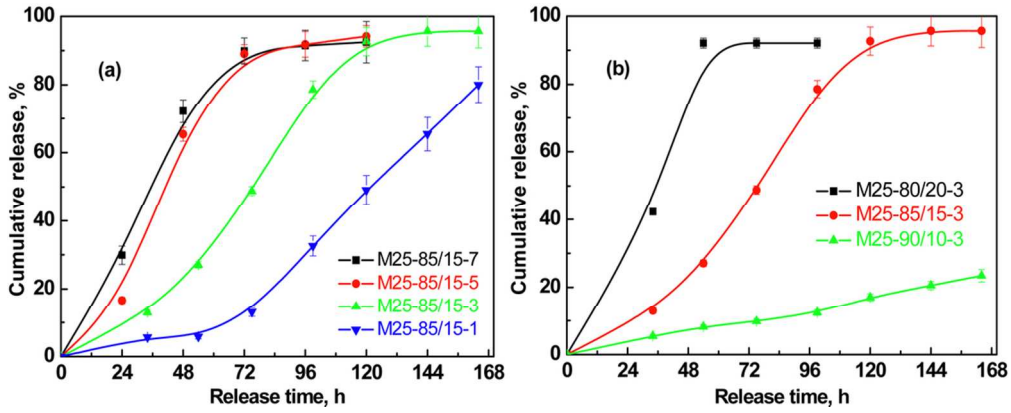

Fig. 10 The release of TI: (a) at different catalysis pH values and (b) at different molar ratios of TEOS and TESPSA
99x39mm (300 x 300 DPI)

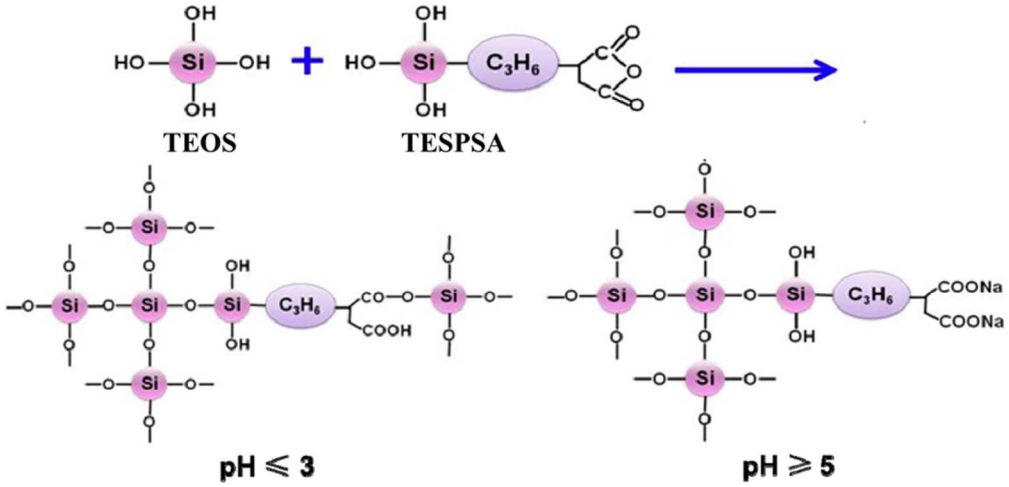

Fig. 11 The formation of co-xerogel at different pH values
73x35mm (300 x 300 DPI)

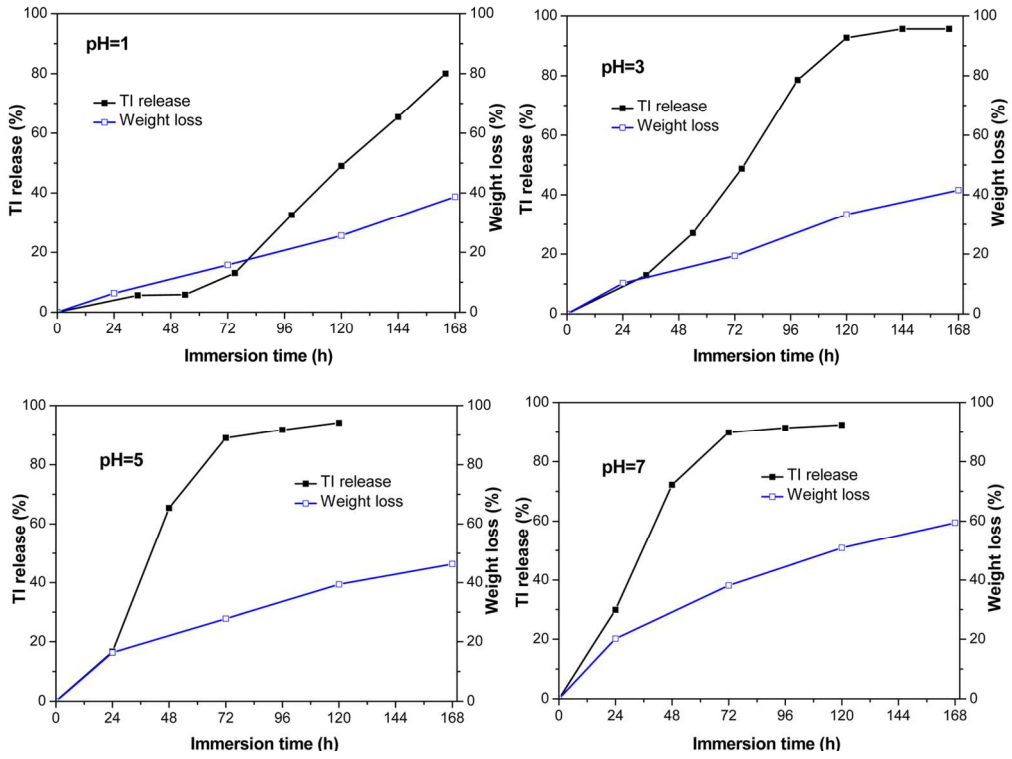

Fig. 12 The combination of weight loss and TI release data
132x98mm (300 x 300 DPI)

Tables

Table 1 Synthesis parameters for pure co-xerogel and TI loaded co-xerogel

Specimen	Molar ratio of TEOS/TESPSA	TEOS, ml	TESPSA g	DI water, ml	1N HCl, ml	TI solution (10mg/ml), ml	TI loading, mg/g xerogel	pH
M-80/20-3	80/20	1	0.3408	0.6	0.067	/	/	2.9
M-85/15-1	85/15	1	0.2406	0.6	0.067	/	/	1.0
M-85/15-3	85/15	1	0.2406	0.6	0.067	/	/	3.4
M-85/15-5	85/15	1	0.2406	0.6	0.067	/	/	5.1
M-85/15-7	85/15	1	0.2406	0.6	0.067	/	/	6.9
M-90/10-3	90/10	1	0.1515	0.6	0.067	/	/	3.1
M25-80/20-3	80/20	1	0.3408	0.6	0.067	1.213	25	3.0
M25-85/15-1	85/15	1	0.2406	0.6	0.067	1.054	25	1.2
M25-85/15-3	85/15	1	0.2406	0.6	0.067	1.054	25	3.2
M25-85/15-5	85/15	1	0.2406	0.6	0.067	1.054	25	5.2
M25-85/15-7	85/15	1	0.2406	0.6	0.067	1.054	25	6.9
M10-85/15-3	85/15	1	0.2406	0.6	0.067	0.422	10	3.1
M50-85/15-3	85/15	1	0.2406	0.6	0.067	2.108	50	3.1
M25-90/10-3	90/10	1	0.1515	0.6	0.067	0.912	25	3.0

Table 2 Specific surface area (SA) and pore volume (PV) for co-xerogel with different molar ratio of TEOS/TESPSA and pH value, based on N_2 adsorption analysis

Specimen	Specific surface area (SA), m^2/g	Pore volume (PV), cc/g
M-85/15-3	1.3	0.001
M-85/15-7	4.7	0.003
M-80/20-3	3.2	0.004
M-85/15-3, after immersed for 7 d	8.1	0.005

Table 3 Weight loss of co-xerogel after 7 days immersion, with different molar ratio of TEOS and TESPSA, and different pH value.

Specimen	Weight loss, %
M-80/20-3	87.9 ±3.3
M-85/15-1	38.7 ±1.8
M-85/15-3	41.6 ±2.0
M-85/15-5	46.3 ±2.3
M-85/15-7	59.5 ±1.9
M-90/10-3	21.7 ±1.9

Table 4 The FTIR spectra vibration modes of anhydride group for co-xerogels synthesized at different pH

Group and vibration		Wavenumber (cm^{-1})	Specimen			
			M-85/15-1	M-85/15-3	M-85/15-5	M-85/15-7
anhydride	symmetric	1710	N	N	N	N
	asymmetric	1810	N	N	N	N
C=O from COO^-	symmetric	1580	N	N	Y	Y
	asymmetric	1420	N	N	Y	Y
C=O from COOH or COO-Si	stretching	1720	← Decrease with the decrease of pH			

N: No appearance in the FTIR curve

Y: Appearance in the FTIR curve

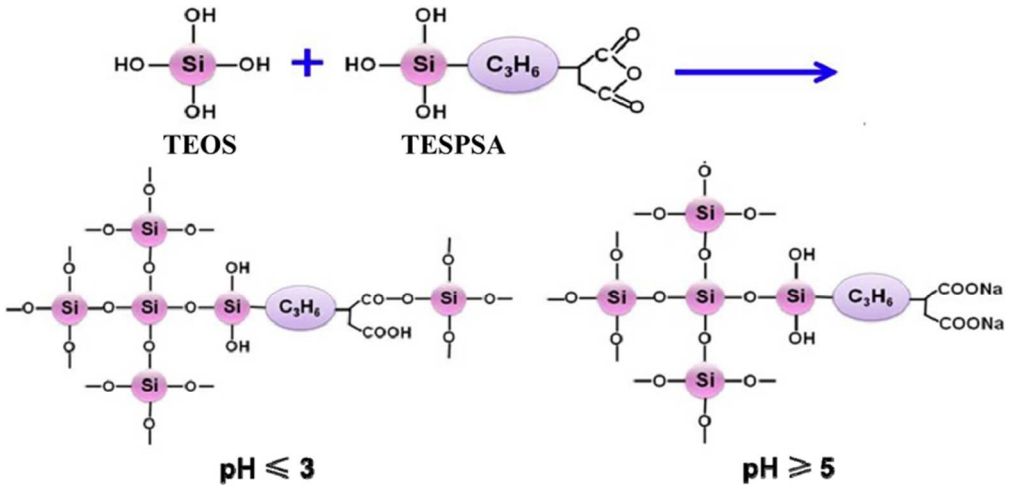

The controlled release of large molecules (such as proteins) in a very short time (several days) was achieved, through the co-hydrolysis and co-condensation of different precursors.
73x35mm (300 x 300 DPI)